Localized Quantum Chemistry on Quantum Computers

Matthew Otten,[1,*] Matthew R. Hermes,[2] Riddhish Pandharkar,[2] Yuri Alexeev,[3] Stephen K. Gray,[4,†] and Laura Gagliardi[5,‡]

[1]*HRL Laboratories, LLC, 3011 Malibu Canyon Road, Malibu, CA 90265*
[2]*Department of Chemistry, Pritzker School of Molecular Engineering, James Franck Institute, Chicago Center for Theoretical Chemistry, University of Chicago, Chicago, IL 60637, USA.*
[3]*Computational Science Division, Argonne National Laboratory, Lemont, IL 60439, USA*
[4]*Center for Nanoscale Materials, Argonne National Laboratory, Lemont, IL 60439, USA*
[5]*Department of Chemistry, Pritzker School of Molecular Engineering, James Franck Institute, Chicago Center for Theoretical Chemistry, University of Chicago, Chicago, IL 60637; Argonne National Laboratory, Lemont, IL 60439, USA.*

(Dated: March 7, 2022)

Quantum chemistry calculations of large, strongly correlated systems are typically limited by the computation cost that scales exponentially with the size of the system. Quantum algorithms, designed specifically for quantum computers, can alleviate this, but the resources required are still too large for today's quantum devices. Here we present a quantum algorithm that combines a localization of multireference wave functions of chemical systems with quantum phase estimation (QPE) and variational unitary coupled cluster singles and doubles (UCCSD) to compute their ground state energy. Our algorithm, termed "local active space unitary coupled cluster" (LAS-UCC), scales linearly with system size for certain geometries, providing a polynomial reduction in the total number of gates compared with QPE, while providing accuracy above that of the variational quantum eigensolver using the UCCSD ansatz and also above that of the classical local active space self-consistent field. The accuracy of LAS-UCC is demonstrated by dissociating $(H_2)_2$ into two H_2 molecules and by breaking the two double bonds in *trans*-butadiene and resources estimates are provided for linear chains of up to 20 H_2 molecules.

arXiv:2203.02012v1 [quant-ph] 3 Mar 2022

I. INTRODUCTION

Chemical systems with many close-lying electronic states or, more generally, strongly correlated electrons pose a significant challenge for modern electronic structure theories in computational quantum chemistry[1–5]. When transition metals or heavier elements are involved, degenerate and nearly degenerate electronic states are common, and single-reference electronic structure methods such as Kohn–Sham density functional theory often fail[6–8]. In these situations one has to use multireference methods to generate multiconfigurational wave functions and accurately describe these near degeneracies[9–11].

Scientists also want to compute properties of large chemical systems or solids with accurate quantum chemistry methods, in spite of steep computational requirements. One way to achieve such computations is to use fragmentation methods. Many variations of fragmentation methods exist[12–15], but the common feature is that a large molecular system is divided into fragments and quantum-mechanical calculations are performed on the fragments. An especially important case is the application of fragmentation methods to multireference wave functions because of the exponential explosion of the computational cost with respect to the size of the active space of electronic configurations.

In the complete active space self-consistent field (CASSCF) method[16], all the electronic configurations that can be formed for a given number of active electrons distributed in a given number of active orbitals are included in the wave function. Thus, the wave function scales exponentially with the number of active electrons and orbitals, and the method has only limited application to chemically relevant systems. If one wants to study systems containing, for example, several transition metals[17–21], the active site of a protein[22], or extended organic chains in their ground and excited states[22,23], more affordable multireference methods have to be developed. This is one of the major challenges of modern electronic structure theory.

Reducing the computational cost of CASSCF or other multiconfiguration self-consistent field calculations is pursued both in the development of new well-motivated theoretical approximations and in the application of new developments in computational hardware[24,25]. On the theoretical side, one strategy is to identify subspaces of the CAS that can be treated on different footings[26,27] or interact with one another only weakly[28–32]. The localized active-space self-consistent field (LASSCF) method[33–36], also known as the cluster mean-field (cMF) method,[37] is an example of such a strategy. LASSCF is designed for applications in which electrons are strongly correlated in different weakly interacting physical regions of a molecule and approximates the strongly correlated part of the wave function as a single antisymmetrized product of subspace wave functions. The computational cost of LASSCF is a linear function of the number of such unentangled subspaces.

Some of the authors have recently shown that LASSCF accurately reproduces the CASSCF spin-state energy gaps of bimetallic compounds and the simultaneous dissociation of two double bonds in bisdiazene at a significantly reduced cost[34,35]. However, LASSCF fails to recover any electron correlation between fragments, for example in the *cis-trans* isomerization of stilbene and similar systems[36]. Moreover, methods to restore the missing correlation variationally[38], perturbatively[37,39], or *via* the coupled-cluster (CC) approach[40] on classical computers must usually enumerate a general many-body basis for each fragment. That is, they inherit the complications of multireference perturbation and CC theory[10,41] over traditional single-reference perturbative or truncated coupled-

cluster (CC) corrections based on second quantization[42,43].

Recently, the development of quantum computers has led to an increased interest in novel quantum algorithms, especially for computational quantum chemistry, which is widely seen as a potential "killer app" of quantum computers[44–46]. The quantum phase estimation (QPE) quantum algorithm[47] can potentially offer exponential speedups when large fault-tolerant quantum computers are available[48,49], under the assumption that an initial state with non-negligible overlap can be prepared[50,51]. Additionally, the variational unitary coupled cluster (UCC) requires only a polynomial number of gates to represent on a quantum computer, whereas representing the same ansatz classically has no known polynomial solution[52,53]. For the noisy, intermediate-scale quantum (NISQ)[54] devices that we have today, these algorithms are not tenable, since they require coherence times far beyond what is available. Variational algorithms, such as the variational quantum eigensolver (VQE)[53], have been used to perform calculations of the ground state energy of small molecules, with limited accuracy, on NISQ devices[55–57]. Quantum algorithms that have less stringent requirements compared with full QPE, and at the same time accuracy beyond that demonstrated by variational algorithms such as VQE, will be required to productively use the progressively larger and higher-quality quantum devices as they become available in the next few years.

In this paper we describe a framework for such quantum algorithms, inspired by classical LASSCF. The wave function within a fragment is solved by using one method (e.g., QPE), and correlation between fragments is encoded variationally by using an ansatz that entangles the fragments. This approach goes beyond what can be achieved with classical fragment methods, such as LASSCF, by providing additional correlation between fragments, while significantly reducing the total computational time (estimated via the number of gates) compared with full QPE.

II. THEORY

A. Multireference Methods with Exponential Scaling

We seek to find the ground state of the second-quantized molecular Hamiltonian for a given number of M electrons,

$$\hat{H} = h_q^p \hat{a}_p^\dagger \hat{a}_q + \frac{1}{4} h_{qs}^{pr} \hat{a}_p^\dagger \hat{a}_r^\dagger \hat{a}_s \hat{a}_q, \tag{1}$$

where $\hat{a}_p^\dagger$ ($\hat{a}_p$) creates (annihilates) an electron in spin orbital p; h_q^p and h_{qs}^{pr} are the one- and antisymmetrized two-electron Hamiltonian matrix elements, respectively; and repeated internal indices are summed. Generally, for N spin orbitals, $\hat{H}$ has a sparse-matrix representation in a space of size $O\binom{N}{M}$ and has $O(N^4)$ elements. Full-configuration interaction (FCI) determines the exact energy within a given one-electron basis set (the FCI energy) at exponential cost. Methods such as CASSCF (and its restricted[26,27] and generalized[28,58] active space approximations) or selected configuration interaction[59,60], can go beyond FCI in system size, maintaining comparable accuracy, but still scale exponentially. The density matrix renormalization group[61–64] and coupled cluster methods[43] can scale polynomially but introduce (sometimes uncontrollable) approximation errors. Here we briefly describe the LASSCF algorithm[33,35], which will serve as the basis for our fragment-based quantum algorithms.

B. LASSCF

In LASSCF, the wave function of a molecule is approximated as

$$|\mathrm{LAS}\rangle = \bigwedge_K |\Psi_K\rangle \wedge |\Phi\rangle, \tag{2}$$

where $|\Psi_K\rangle$ is a general many-body wave function describing M_K electrons occupying N_K active orbitals of the Kth "fragment" or "active subspace," $|\Phi\rangle$ is a single determinant spanning the complement of the complete active space, and the wedge operator ("$\wedge$") implies an antisymmetrized product.

In the variational[35] implementation of LASSCF, this wave function is obtained by minimizing the LAS energy,

$$E_{\mathrm{LAS}} = \langle \mathrm{LAS}|\hat{H}|\mathrm{LAS}\rangle, \tag{3}$$

with respect to all orbital rotations and configuration interaction (CI) vectors defining $|\mathrm{LAS}\rangle$. This is accomplished by introducing a unitary operator (see the Supporting Information of Ref. 35) that is parameterized in terms of all nonredundant transformations of the orbitals and CI vectors,

$$|\mathrm{LAS}\rangle \to \hat{U}_{\mathrm{orb}} \prod_K \hat{U}_{\mathrm{CI},K} |\mathrm{LAS}\rangle, \tag{4}$$

where

$$\hat{U}_{\mathrm{orb}} = \exp\left\{x_l^k \left(\hat{a}_k^\dagger \hat{a}_l - \hat{a}_l^\dagger \hat{a}_k\right)\right\}, \tag{5}$$

$$\hat{U}_{\mathrm{CI},K} = \exp\left\{x_{\vec{k}} \left(|\vec{k}\rangle\langle\Psi_K| - |\Psi_K\rangle\langle\vec{k}|\right)\right\}, \tag{6}$$

where k, l index individual spin orbitals in two different subspaces (including the inactive and virtual subspaces outside of the CAS) and where $|\vec{k}\rangle$ is a determinant or configuration state function. First and second derivatives of Eq. (3) with respect to the generator amplitudes (x_l^k and $x_{\vec{k}}$) are obtained by using the Baker–Campbell–Hausdorff (BCH) expansion, and the energy is minimized by repeated applications of the preconditioned conjugate gradient (PCG) method[65,66].

The orbital unitary operator, $\hat{U}_{\mathrm{orb}}$, corresponds to the UCC correlator truncated after the first ("singles") term:

$$\hat{U}_{\mathrm{UCC}} \equiv \exp\left\{\hat{T}_{\mathrm{UCC}}\right\}, \tag{7}$$

$$\hat{T}_{\mathrm{UCC}} \equiv x_l^k \left(\hat{a}_k^\dagger \hat{a}_l - \mathrm{h.c.}\right) + \frac{1}{4} x_{ln}^{km} \left(\hat{a}_k^\dagger \hat{a}_m^\dagger \hat{a}_n \hat{a}_l - \mathrm{h.c.}\right) + \ldots. \tag{8}$$

The use of the more general cluster operator, Eq. (8), in place of the orbital rotation unitary operator, Eq. (5), corresponds to a multireference unitary coupled cluster method[67] built on top of a $|\mathrm{LAS}\rangle$ reference wave function. Such a method is expected to more flexible than LASSCF itself, in

that doubles and higher-order cluster amplitudes could encode electron correlation and entanglement between active subspaces. This would require the reference wave function, $|\mathrm{LAS}\rangle$, to be updated by explicit exponentiation of the general cluster operator, Eq. (8), after each execution of the PCG algorithm. On classical computer hardware, however, this is not an efficient way to extend LASSCF.

C. LAS Methods on Quantum Computers

Here we describe an algorithm for molecular calculations that goes beyond the limited accuracy of standard VQE[56,57], while having dramatically reduced computational complexity compared with QPE [see Methods section]. The algorithm exploits the structure of the molecule by separating it into coupled fragments, as is done in the classical algorithm, LASSCF. The quantum algorithm, however, goes beyond classical LASSCF by providing some degree of entanglement between the fragments.

The algorithm begins by segmenting the orbital active space of a given molecule into distinct fragments defined by non-overlapping orbital subspaces, as in classical LASSCF. For instance, orthogonalized atomic orbitals generated by using the meta-Löwdin method[68] can be sorted into localized fragments and then projected onto a guess for the CAS of a given molecule to produce localized active orbitals. We construct an effective Hamiltonian that omits non-mean-field interfragment interactions, resulting in a sum of local fragment Hamiltonians,

$$\hat{H}_{\mathrm{eff}} = \sum_{K}^{n_f} \left(\tilde{h}^{k_1}_{k_2} \hat{a}^\dagger_{k_1} \hat{a}_{k_2} + \frac{1}{4} h^{k_1 k_3}_{k_2 k_4} \hat{a}^\dagger_{k_1} \hat{a}^\dagger_{k_3} \hat{a}_{k_4} \hat{a}_{k_2} \right), \tag{9}$$

where $k_1, k_2, \ldots$ index distinct active orbitals of the Kth fragment and where

$$\tilde{h}^{k_1}_{k_2} = h^{k_1}_{k_2} + h^{k_1 i}_{k_2 i} + \sum_{L \neq K} h^{k_1 l_1}_{k_2 l_2} \gamma^{l_1}_{l_2}, \tag{10}$$

where i and l_n index respectively inactive orbitals [i.e., those defining $|\Phi\rangle$ in Eq. (2)] and active orbitals of the Lth fragment and where $\gamma^{l_1}_{l_2}$ is a one-electron reduced density matrix element for spin orbitals l_1 and l_2,

$$\gamma^{l_1}_{l_2} \equiv \langle \mathrm{LAS} | \hat{a}^\dagger_{l_1} \hat{a}_{l_2} | \mathrm{LAS} \rangle = \langle \Psi_L | \hat{a}^\dagger_{l_1} \hat{a}_{l_2} | \Psi_L \rangle . \tag{11}$$

Given a set of localized active orbitals that minimize the LASSCF energy, if the density matrices in Eq. (10) are obtained from a classical LASSCF calculation on the same system, then the QPE algorithm applied to $\hat{H}_{\mathrm{eff}}$ generates the active-space part of the LASSCF wave function, $|\mathrm{QLAS}\rangle = \bigwedge_K |\Psi_K\rangle$, on the quantum computer. The same result is achieved if density matrices are obtained self-consistently from the QPE evaluation. If the density matrices are obtained in some other way, for instance from $|\mathrm{HF}\rangle$, then an approximation to the LASSCF wave function is obtained.

The QPE step provides the initial $|\mathrm{QLAS}\rangle$ for each fragment step by repeating the measurement of the phase until it is consistent with the phase representing the ground state energy, which collapses the system into the ground state wavefunction. This introduces some overhead, as each fragment will need to be in the ground state to continue to the next step. Furthermore, a full QPE solve, estimating the ground state energy, must be performed initially to provide a comparison value.

A sequence of UCC with singles and doubles (UCCSD) circuits, with variable parameters, is then applied across m fragments each (which we term m-local), leading to the LAS-UCC wave function,

$$|\mathrm{QLAS}(\boldsymbol{x})\rangle \rightarrow \prod_{\zeta} \hat{U}_{\mathrm{UCCSD},\zeta}(\boldsymbol{x}) \, |\mathrm{QLAS}\rangle , \tag{12}$$

where $\hat{U}_{\mathrm{UCCSD},\zeta}(\boldsymbol{x})$ is the UCCSD ansatz including only creation/annihilation operators within the m fragments that it spans, ζ is a list of fragment indices of size m, and $\boldsymbol{x}$ are the associated singles and doubles cluster amplitudes. The factorization of Eq. (8) implied by Eq. (12) is based on the intuition that physically adjacent active subspaces are likely to be more strongly entangled to one another than subspaces on opposite ends of a large molecule. The parameters of the UCCSD circuit are varied to minimize the total energy of the full system, as in VQE [see also Methods section]:

$$E = \min_{\boldsymbol{x}} \langle \mathrm{QLAS}(\boldsymbol{x}) | \hat{H} | \mathrm{QLAS}(\boldsymbol{x}) \rangle . \tag{13}$$

A schematic representation of the described circuit is shown in Fig. 1. This provides electron correlation between the fragments, in a way that scales exponentially on classical computers, but only polynomially on quantum computers. Moreover, this procedure provides a better estimate of the ground state energy than the product wave function or the UCCSD would provide alone. Note that, unlike LASSCF, this method is not strictly variational (despite the use of VQE) because the initial product-state wave function, $\bigwedge_K |\Psi_K\rangle$, is not variationally reoptimized in the presence of the UCCSD correlators. The QPE circuits could also be replaced with a local variational ansatz, leading to a fully variational algorithm, which we term LAS-VQE and describe in the Supplementary Information.

To understand the large improvement in computational complexity of our approach, we focus on a system of n_f fragments, with the number of orbitals per fragment, N_K, constant as the number of fragments grows. The total system size is defined by $N = N_K n_f$ orbitals. We also assume that each fragment interacts with only the m geometrically nearest fragments and that m does not grow with n_f. These are reasonable assumptions for many interesting molecules and mirror the assumptions made in classical LASSCF. Under these assumptions, the QPE solver for the unentangled fragments does not grow with N, since N_K is assumed to be fixed while n_f grows. The number of small QPE sections grows linearly with

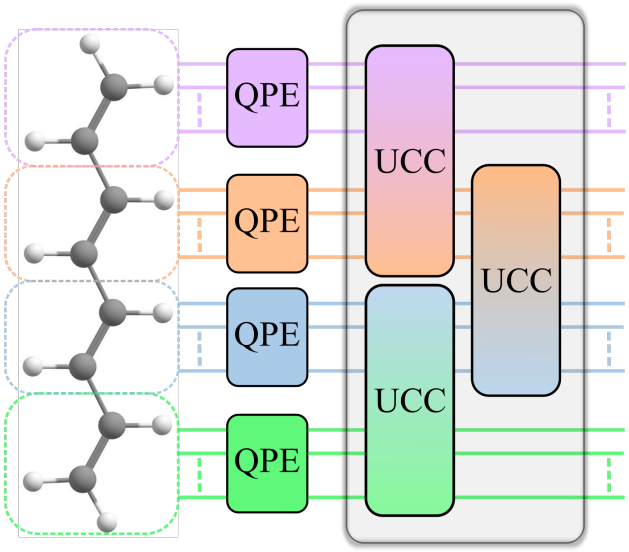


FIG. 1. Diagram of example circuit using LAS-UCC. The system of interest is first separated into distinct fragments. QPE is used on each fragment to solve for the approximate unentangled ground state. Correlation between fragments is then added in, variationally, through a unitary coupled cluster ansatz.

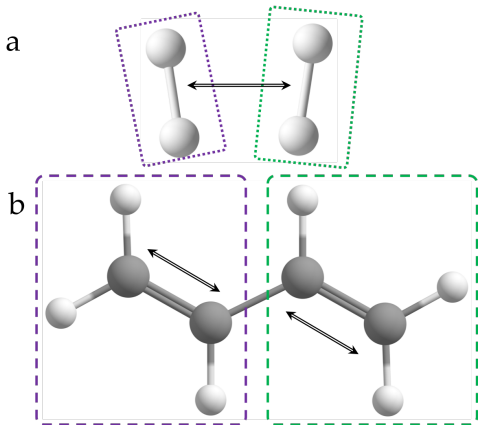


FIG. 2. Two model systems used for testing. (a) The asymmetric hydrogen dimer, $(H_2)_2$. Each H_2 molecule is a fragment described by a 2-electron, 2-spatial orbital or (2,2) active subspace in the dimer's LAS wave function. The potential energy surface is scanned along the distance between the two H_2 bond midpoints, indicated by the black double line. (b) The *trans*-butadiene molecule at its CASSCF(8,8)/6-31G ground-state equilibrium geometry. Dashed boxes depict the two notional fragments containing the two (4,4) active subspaces in the LAS wave function. Black double lines indicate the internal coordinate along which the potential energy surface is scanned; the two terminal methylene units are simultaneously removed from the central acetylene unit.

the number of fragments, of course. Typically, the Jordan–Wigner transformation would introduce an $O(N)$ term to enforce the anticommutation relations among the orbital creation and annhilation operators. However, in the case of linear chains, as we study here, ordering the orbitals such that all up and down occupied and virtual orbitals in a given fragment are close, the high-weight Z part of the Jordan–Wigner transformation effectively cancels out, causing no scaling with total number of orbitals. See Supplementary Information for more details. Together, this leads to an overall $O(n_f N_K^4) \approx O(N)$ (linear) number of gates to solve for the n_f unentangled product wave functions. The UCCSD correlator, which is then applied, has $O(m^4 N_K^4)$ terms in the cluster operator for each correlator, because the UCCSD circuit spans only m fragments. Neither m nor N_K grows with the total size (number of spin orbitals) of the system, N. The number of m-local correlators grows as $O(n_f)$. Again, by careful ordering of the orbitals, the Jordan–Wigner transformation does not introduce any scaling overhead. The complexity of the m-local UCCSD correlator is then $O(n_f m^4 N_K^4) \approx O(N)$ (linear). This creates an overall linear scaling in the number of gates for linear chain geometries, with respect to only the total size of the system, N, and is polynomially ($O(N^4)$) better than performing QPE alone, while providing accuracy above VQE using the UCCSD ansatz and classical LASSCF. Many of the gates can be done in parallel, such as the local QPE circuits and the different m-local UCCSD correlators, leading to an expected overall sub-linear depth. If the fragments are coupled in a geometry more complicated than a linear chain, the UCCSD correlator will potentially incur the $O(N)$ Jordan-Wigner overhead, leading to an overall $O(N^2)$ scaling for arbitrary geometries with an expected $O(N)$ depth.

D. Illustrative Molecular Systems

In the calculations discussed below, we consider two systems, depicted in Fig. 2. The first, shown in Fig. 2(a), is a simplistic model of weakly interacting fragments, consisting of two H_2 molecules at various distances between their two midpoints using a minimal STO-3G atomic orbital (AO) basis set, and the two active subspaces in the LAS wave function correspond to the active spaces of the two H_2 molecules. We use this small basis set because of the size limitations of today's quantum computers and simulations. The bond lengths and internal angles of this system are set arbitrarily to remove point group symmetry so that differences between various methods are not obscured by the simplicity of a symmetrized electronic wave function. The interaction between the two fragments in this model system are weak, and the LAS wave function is therefore expected to provide an excellent model of the FCI wave function except when the distance between the two molecules is very small. We additionally extend this system up to 20 H_2 in a linear chain, where we estimate only the total number of quantum resources necessary.

The second system, depicted in Fig. 2(b), is the *trans*-butadiene molecule. The potential energy surface of this molecule is scanned along the internal coordinate corresponding to the simultaneous stretching of both the C=C double bonds, leading to the removal of two methylene units from a central C_2H_2 (distorted acetylene-like) unit. In the LAS wave function, the molecule is divided into two fragments split across the central C–C bond, and each fragment is described by a (4,4) active subspace. Several molecular orbitals

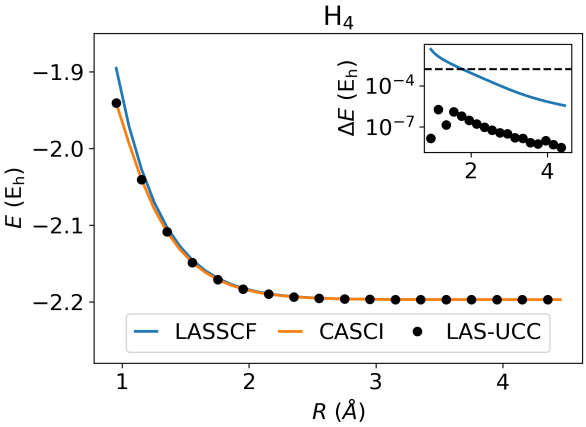


FIG. 3. Energies for $(H_2)_2$ calculated by CASCI, LASSCF, and LAS-UCC. The inset shows the error, with respect to CASCI, of LASSCF and LAS-UCC. The black dashed line represents chemical accuracy. LAS-UCC is able to obtain chemical accuracy, with respect to CASCI, at all distances. LASSCF cannot obtain chemical accuracy at sufficiently short distances.

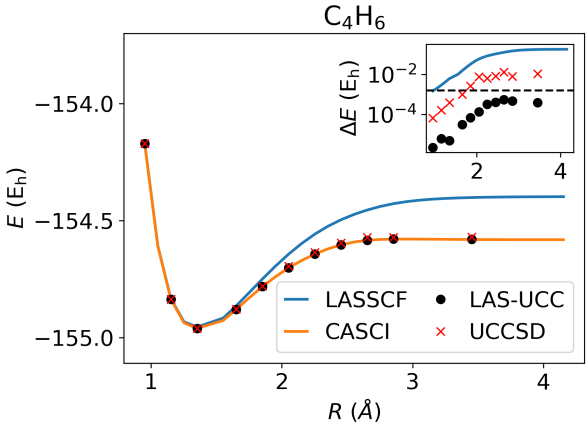


FIG. 4. Energies for C_4H_6 calculated by CASCI, LASSCF, and LAS-UCC. The inset shows the error, with respect to CASCI, of LASSCF and LAS-UCC. The black dashed line represents chemical accuracy. LAS-UCC obtains chemical accuracy across the potential energy surface, whereas LASSCF, which cannot accurately represent the correlation between the fragments, fails to obtain chemical accuracy for most points.

are therefore left inactive, described by an unfragmented single determinant. We employed the 6-31G AO basis set in this case.

The *trans*-butadiene system is a chemical model of the case of two strongly interacting units in a system, where the value of the stretching internal coordinate is a proxy for the strength of electron correlation. Near the equilibrium geometry, dividing the active space into two fragments is chemically reasonable: each fragment encloses one π-bond, and inasmuch as electron correlation affects the system at all, it is a reasonable approximation to consider it only locally. However, as the C=C double bonds are elongated, electrons from the two broken π bonds recouple across the central C_2H_2 unit, which spans the fissure between the two LAS fragments. The LAS wave function cannot model a π bond in this position, and the LASSCF method breaks down.

III. RESULTS AND DISCUSSION

A. LAS-UCC

We demonstrate the efficacy of our framework by simulating the two benchmark molecules, $(H_2)_2$ and *trans*-butadiene, described above. We compare three methods: LASSCF, CAS configuration interaction in the basis of LASSCF orbitals (CASCI), and our new algorithm, LAS-UCC. LASSCF represents the best unentangled set of wave functions and is equivalent to the solution after the QPE circuits but before the use of the UCCSD ansatz. Note that CASCI is slightly different from CASSCF since the orbitals are not variationally reoptimized. CASCI solves for the FCI wave function within the active space; in this case, it is equivalent to using QPE across the whole molecule and represents the reference result in these studies.

Figure 3 shows the results of applying the methods to the hydrogen dimer as the two H_2 molecules are pulled apart. We see that LASSCF, CASCI, and LAS-UCC agree except for very small distances where LASSCF no longer provides accurate energies.

Figure 4 shows the results for *trans*-butadiene, a model of strongly correlated fragments. Here, as the terminal methylene units are removed, the interfragment correlation grows as a double bond is formed between the fragments. The UCCSD ansatz can accurately represent this level of entanglement, allowing LAS-UCC to achieve nearly CASCI accuracy, whereas LASSCF fails to account for this entanglement. With a standard Hartree-Fock initial state, as is typically done in VQE, the UCCSD ansatz is unable to obtain chemical accuracy for the large distances. We also attempted to use the so-called 'hardware-efficient' ansatz[57], but were unable to obtain results significantly better than Hartree-Fock using depths up to 10 (which corresponds to a similar number of parameters as the UCCSD ansatz) at equilibrium.

B. Resource Estimates

To demonstrate the scaling advantage of our method, we perform resource estimation for the number of logical quantum gates necessary for several different quantum algorithms: the QPE algorithm over the full unfragmented molecule; the UCCSD ansatz over the full unfragmented molecule; and the two steps of our proposed LAS-UCC method, the fragmented QPE and the 2-local UCCSD (which corresponds to the circuit depicted in Fig. 1). We estimate the number of resources needed for the QPE algorithm if only a single Trotter time step

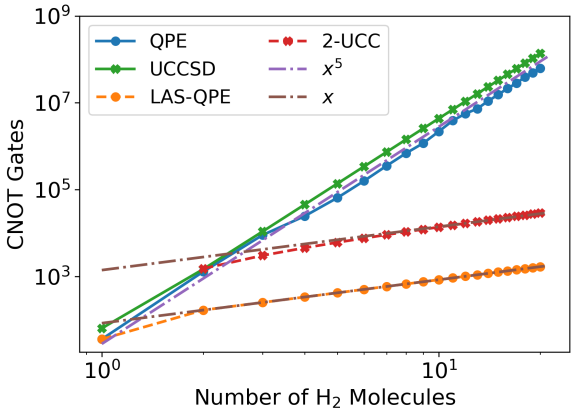


FIG. 5. Estimated two-qubit gate counts using various algorithms. The QPE estimates assume only a single Trotter step; $O(1000)$ will need to be taken to obtain chemical accuracy. Polynomials of various orders have been plotted to demonstrate the scaling. Our algorithm, LAS-UCC, requires both the LAS-QPE and 2-UCC circuits and thus has an overall $O(N)$ scaling, compared with the $O(N^5)$ scaling of UCC and QPE.

were needed; $O(1000)$ time steps will be needed for typical systems to get to chemical accuracy[46,69]. Note that these estimates represent only the number of two-qubit CNOT gates, which we use as a primary gauge of the number of total resources. Single-qubit gates are also necessary; the estimates for these resources can be found in the Supplementary Information and scale similarly to the number of CNOT gates. We also note here that we are only comparing the scaling number of gates; QPE, with a sufficiently good initial state and enough Trotter states, will of course be the most accurate of all compared algorithms.

We use a model system of an increasing number of H_2 molecules and look at how the number of CNOT gates increases as the number of molecules increases, as shown in Fig. 5. As the number of H_2 molecules increases, the number of gates needed for all methods also increases. As predicted in the complexity analysis of QPE [see Methods section], the total number of gates for a single Trotter step in the QPE algorithm grows as $O(N^5)$. Similarly, the number of gates needed for a global UCCSD ansatz also grows as $O(N^5)$, as expected[56]. This result is compared with the much smaller number of gates necessary to implement the two steps of our LAS-UCC algorithm. As expected, both the QPE and UCCSD parts of LAS-UCC provide dramatic scaling advantages, with the 2-local UCCSD ansatz and the QPE of the reduced Hamiltonian both scaling as only $O(N)$. We note that, in addition to evaluating the quantum circuits here, an additional optimization loop is needed when using the UCCSD ansatz, whether it is global or 2-local. Using a 2-local UCCSD ansatz also greatly reduces the number of parameters that need to be optimized compared with a global UCCSD ansatz.

C. Discussion

Here we compare LAS-UCC with the two quantum algorithms that it is composed of: QPE and variational UCCSD. Compared with global QPE, LAS-UCC reduces the total quantum resource cost by approximating the system with non-interacting fragments and adding in some interaction between fragments (those described by a UCCSD ansatz spanning the fragments). This in general reduces the accuracy; but as shown in the preceding sections, LAS-UCC provides accuracy comparable to CASCI (and therefore global QPE) for the systems considered here. The *trans*-butadiene molecule is a model for larger, more complicated systems of strongly interacting units. Many single molecular magnets have such pockets of strong correlation localized on the metal centers, which moderately interact with each other[70,71]. With LAS-UCC we not only can obtain the wave function efficiently but also can selectively couple the fragments with the UCC correlator, offering further insight into the nature of these interactions. Affordable and accurate modeling of phenomena such as singlet fission[72,73] in molecular crystals of conjugated organic compounds can be performed with LAS-UCC, as fault-tolerant quantum computers become available. This approach will also be used to study chemical processes involving inter-fragment bond formation and breaking while still treating all points on a potential energy surface at comparable footing.

Compared with standard UCCSD, LAS-UCC can be seen as augmenting UCCSD with a multireference initial state. Instead of using single-determinant Hartree–Fock, as is standard in VQE demonstrations of UCCSD[57,74–77], LAS-UCC uses the unentangled product state of the ground state wave functions of each fragment (which is also the LASSCF wavefunction). This provides additional accuracy, above standard single-reference UCCSD, at a negligible increase in cost. When using a global UCCSD ansatz, the increase in the number of gates is negligible, even when taking into account the $O(1000)$ time steps that would be needed to implement the QPE step. Using the m-local ansatz provides further reduction. There have been other proposals for preparing interesting, multireference initial state in context of efficiently finding states with large overlap with the true ground state[78,79]. These algorithms could be used in-place of the QPE part of LAS-UCC to provide the initial state and potentially adapted to give similar LASSCF-like states with similar overhead reductions as shown for QPE.

Moreover, recent advances in VQE algorithms have developed various ways to reduce the cost associated with the UCC correlator[44,46,80–83]. As presented in the Theory section, LAS-UCC can also be seen as a post-LASSCF method that recouples select fragments at a level of theory beyond the mean field. The addition of the doubles or higher terms in the cluster operator provides a way to systematically improve the accuracy beyond the LASSCF reference. On classical computers, such an approach requires truncating[67] or approximating[84] the non-terminating BCH expansion in a more or less arbitrary way.

Not every system will be accurately described by LAS-UCC, of course, but one can systematically increase the accu-

racy in several ways, while increasing the total resource cost. Increasing the size of each fragment (which in turn decreases the number of fragments) gradually increases the accuracy, until the limit of a single fragment, where the UCCSD ansatz becomes redundant and the algorithm becomes simply global QPE. On the UCC side, the order of the ansatz can be increased. Triples, quadruples, and so on can be included at increasing cost. If using an m-local ansatz, the scaling is unaffected, but the total number of gates increases. The locality of the ansatz, m, can also be increased, providing explicit correlation between more geometrically distant fragments.

IV. CONCLUSIONS

We introduced LAS-UCC, a quantum algorithm that combines a fragmentation of the wave function of a chemical system with QPE and variational UCCSD to compute the ground state energy of such a system. LAS-UCC can describe compounds containing strongly interacting fragments, and it provides a polynomial scaling advantage in the number of quantum gates compared with other quantum algorithms such as QPE and UCCSD. Since the fragments' reduced Hamiltonians have fewer terms and by ensuring the locality of the Jordan-Wigner transform, the overall gate count will be $O(N)$ with respect to the total size of the system N for for linear geometries and $O(N^2)$ more generally, compared with $O(N^5)$ requirements for QPE. We also demonstrated the accuracy of LAS-UCC on $(H_2)_2$ and *trans*-butadiene molecules and performed resource estimations of larger systems to provide evidence for potential scaling advantages.

As larger fault-tolerant quantum computers are developed, we expect that our algorithm will be able to provide accurate calculations of large and useful chemical systems, such as molecular magnets and qubits, photovoltaic materials, and large biomolecules that are out of reach of classical computing algorithms but for which QPE would be too expensive.

V. METHODS

A. Quantum Algorithms

Here we describe two quantum algorithms that serve as the primary components for our fragment-based quantum algorithm.

1. Quantum Phase Estimation

The quantum phase estimation algorithm solves for the eigenvalue, λ_k, for an eigenvector $|v_k\rangle$ of some unitary matrix, U. In addition to its use in quantum chemistry, it forms the basis for many important quantum algorithms, such as Shor's prime number factoring algorithm[85] and the Hassidim–Harrow–Lloyd algorithm for inverting matrices[86]. For quantum chemistry problems, the unitary matrix U is generated by the Hamiltonian, H (eq. (1)), over time steps τ:

$$U|v_k\rangle = e^{-i\hat{H}\tau}|v_k\rangle = e^{i2\pi\phi}|v_k\rangle, \tag{14}$$

and the desired energy is mapped to the phase acquired, $E = -2\pi\phi/\tau$, where units have been chosen such that $\hbar = 1$. By combining real-time evolution of the Hamiltonian, $\hat{H}$, with application of the quantum Fourier transform (QFT)[87], the value of the energy can be obtained in polynomial time using a quantum computer.

The computational complexity of the QPE is directly related to the complexity of implementing the unitary propagator $U = e^{-i\hat{H}\tau}$. Many strategies for implementing U exist, including Trotterization[88,89], Taylorization[90], and qubitization[91]. The Hamiltonian, Eq. (1), has $O(N^4)$ terms, where N is the number of spin orbitals. Each term in the Hamiltonian can be transformed into a Pauli string (that is, a product of Pauli operators X, Y, Z, or I) via one of the many fermion-to-spin transformations, such as the Jordan–Wigner[92], parity[93], and Bravyi–Kitaev[94] transformations. In this work we focus on QPE using Trotterization with the Jordan–Wigner transformation since they serve as standard reference points for the other variations. The complexity of QPE for the Hamiltonian, Eq. (1), using Trotterization with the Jordan–Wigner transformation is $O(N^5)$: N^4 arising from the number of terms in the Hamiltonian and an additional N from the Jordan–Wigner transform. Although QPE can obtain estimates of the ground state energy with only a polynomial number of quantum gates, the overheads are still too large for near-term quantum computers. The success of the QPE algorithm directly depends on the overlap of the initial state (which is often taken to be the Hartree-Fock state) and the true ground state. Realistic estimates, taking into account overheads such as quantum error correction, put the needed number of qubits to perform QPE on interesting molecules in the millions[95–97].

QPE is analogous to a Fourier analysis of a correlation function; and, for a given energy accuracy, ϵ, it requires propagation efforts (maximum times) on the order of $O(1/\epsilon)$[46,69]. Since the circuit depth for evaluating the propagator for individual fragments will naturally be lower than for the full system, the QPEs involved in our LAS approach will be significantly cheaper than full QPE.

2. Variational Quantum Eigensolver

The variational quantum eigensolver is a hybrid quantum-classical algorithm that relies on the variational principle to find an estimate of the ground state energy of a given molecule. A circuit with variable parameters, θ, serves as an ansatz, whose energy is evaluated on a quantum computer and whose parameters are iteratively optimized by a classical computer. For a circuit ansatz $|\psi(\theta)\rangle$, VQE estimates the energy as

$$E = \min_{\theta} \langle\psi(\theta)|\hat{H}|\psi(\theta)\rangle\,. \tag{15}$$

The Hamiltonian, $\hat{H}$, is transformed into a sum of Pauli strings via a fermion-to-spin transformation, and the expectation value of each term is measured from the quantum computer separately and summed on the classical computer. VQE

has much less stringent quantum resource requirements than QPE has, since it offloads much of the work (such as optimization) to the classical computer. Hence, VQE has been used in proof-of-principle calculations for small molecules[74,76,77].

The accuracy of VQE is determined by the quality of the ansatz, $|\psi(\theta)\rangle$. The UCCSD ansatz is an interesting choice as wave function for VQE since there is no known way to efficiently implement UCCSD on classical computers[98–100], but it can be implemented with $O(N^5)$ gates on quantum computers[56,101,102]. The UCCSD ansatz is

$$|\psi_{\mathrm{UCCSD}}\rangle = \hat{U}_{\mathrm{UCCSD}}\,|\mathrm{HF}\rangle = \exp\left\{\hat{T}_{\mathrm{UCCSD}}\right\}|\mathrm{HF}\rangle\,, \qquad (16)$$

where $\hat{T}_{\mathrm{UCCSD}}$ is defined by truncating the more general cluster operator of Eq. (8) at the second term. While the UCCSD ansatz can be implemented on NISQ devices for small molecules[57,75], it is limited in its accuracy because of only including up to doubles excitations.

B. Computational Methods

To calculate the accuracy of the proposed method for small molecules, we use the following strategy. We first use a classical LASSCF solver, as implemented in the *mrh* package[103], to find the best product wave function. This effectively provides an equivalent solution to that of the QPE step of our proposed algorithm. We then represent this product wave function as a CI vector in the complete active Fock space and apply a UCCSD correlator, as well as its derivatives with respect to all amplitudes, to this reference CI vector. We employ the factorization reported by Chen et al.[104] to avoid the BCH expansion and its inevitable approximate truncation. The resulting $|\mathrm{QLAS}\rangle$ CI vector and its derivatives ($|\delta\mathrm{QLAS}\rangle$) with respect to the unitary coupled cluster amplitudes are used to compute the energy, $\langle\mathrm{QLAS}|\hat{H}|\mathrm{QLAS}\rangle$, and its derivatives, $\langle\delta\mathrm{QLAS}|\hat{H}|\mathrm{QLAS}\rangle$. We then minimize the former using the latter and the Broyden—Fletcher-–Goldfarb-–Shanno algorithm. We find that this approach is more efficient than directly simulating the quantum circuits. We note that this method scales exponentially on classical computers.

To provide gate count estimates, we use the Q# package[105], generally following the framework of Ref. 106. The full and reduced Hamiltonians are produced by using the *mrh* package[103], and both Hamiltonians are then passed to the Q# package to estimate the number of CNOT gates using the QPE algorithm with a single Trotter time step for each. Additionally, we estimate the number of CNOT gates necessary to calculate various UCCSD ansatzes, including a global UCCSD ansatz over the whole unfragmented molecule and multiple 2-local ansatzes that span only two fragments. We count only the number of logical quantum gates needed. Real quantum computers will require additional overheads, owing to limited connectivity and the need to use expensive quantum error correction protocols to deal with inevitable errors[96,97]. Furthermore, we provide gate counts only; no attempt was made to count gate depth, which is typically smaller, because many gates can be implemented in parallel.

VI. CONTRIBUTIONS

L.G., S.G. M.O. and M.R.H. designed the project. M.O. wrote the quantum algorithm and tested it. M.R.H. wrote the LASSCF classical code. R.P. tested the codes and performed some of the calculations. Y.A. helped with the theory and suggested testing calculations. M.O. and M.R.H. wrote the initial draft of the manuscript. All authors contributed to the scientific discussions and manuscript revisions.

ACKNOWLEDGMENTS

This research is based on work supported by Laboratory Directed Research and Development (LDRD) funding from Argonne National Laboratory, provided by the Director, Office of Science, of the U.S. DOE under Contract No. DE-AC02-06CH11357. This work was performed, in part, at the Center for Nanoscale Materials, a U.S. Department of Energy Office of Science User Facility, and supported by the U.S. Department of Energy, Office of Science, under Contract No. DE-AC02-06CH11357. MRH and LG are partially supported by the U.S. Department of Energy (DOE), Office of Basic Energy Sciences, Division of Chemical Sciences, Geosciences, and Biosciences under grant no. USDOE/DE-SC002183. This material is based upon work supported by the U.S. Department of Energy, Office of Science, National Quantum Information Science Research Centers. We gratefully acknowledge the computing resources provided on Bebop, a high-performance computing cluster operated by the Laboratory Computing Resource Center at Argonne National Laboratory and University of Chicago Research Computing Center.

* mjotten@hrl.com
† gray@anl.gov
‡ lgagliardi@uchicago.edu

[1] P.-O. Löwdin, Adv. Chem. Phys. , 207 (1958).
[2] C. D. Sherrill, A. Dutta, M. L. Abrams, and J. S. Sears (ACS Publications, 2007).
[3] A. I. Krylov, L. V. Slipchenko, and S. V. Levchenko, in *ACS Symposium Series*, Vol. 958 (Citeseer, 2007) pp. 89–102.
[4] T. Stein, T. M. Henderson, and G. E. Scuseria, J. Chem. Phys. **140**, 214113 (2014).
[5] C. A. Gaggioli, S. J. Stoneburner, C. J. Cramer, and L. Gagliardi, ACS Catal. **9**, 8481 (2019).
[6] F. Neese, Coord. Chem. Rev **253**, 526 (2009).
[7] C. R. Jacob and M. Reiher, Int. J. Quantum Chem. **112**, 3661 (2012).
[8] H. S. Yu, S. L. Li, and D. G. Truhlar, J. Chem. Phys. **145**, 130901 (2016).

[9] P. G. Szalay, T. Muller, G. Gidofalvi, H. Lischka, and R. Shepard, Chem. Rev. **112**, 108 (2012).
[10] J. W. Park, R. Al-Saadon, M. K. MacLeod, T. Shiozaki, and B. Vlaisavljevich, Chem. Rev. **120**, 5878 (2020).
[11] C. J. Cramer, M. Włoch, P. Piecuch, C. Puzzarini, and L. Gagliardi, J. Phys. Chem. A **110**, 1991 (2006).
[12] M. S. Gordon, D. G. Fedorov, S. R. Pruitt, and L. V. Slipchenko, Chem. Rev. **112**, 632 (2012).
[13] M. A. Collins and R. P. Bettens, Chem. Rev. **115**, 5607 (2015).
[14] K. Raghavachari and A. Saha, Chem. Rev. **115**, 5643 (2015).
[15] D. G. Fedorov, Y. Alexeev, and K. Kitaura, J. Phys. Chem. Lett. **2**, 282 (2011).
[16] B. O. Roos, P. R. Taylor, and P. E. M. Siegbahn, Chem. Phys. **48**, 157 (1980).
[17] G. Li Manni, W. Dobrautz, N. A. Bogdanov, K. Guther, and A. Alavi, J. Phys. Chem. A **125**, 4727 (2021).
[18] P. P. Hallmen, H.-J. Werner, D. Kats, S. Lenz, G. Rauhut, H. Stoll, and J. van Slageren, Phys. Chem. Chem. Phys. **21**, 9769 (2019).
[19] P. Sharma, D. R. Pahls, B. L. Ramirez, C. C. Lu, and L. Gagliardi, Inorg. Chem. **58**, 10139 (2019).
[20] R. W. Hogue, S. Singh, and S. Brooker, Chem. Soc. Rev. **47**, 7303 (2018).
[21] J. P. Malrieu, R. Caballol, C. J. Calzado, C. de Graaf, and N. Guihery, Chem. Rev. **114**, 429 (2014).
[22] D. S. Levine, D. Hait, N. M. Tubman, S. Lehtola, K. B. Whaley, and M. Head-Gordon, J. Chem. Theory Comput. **16**, 2340 (2020).
[23] P. Sharma, V. Bernales, S. Knecht, D. G. Truhlar, and L. Gagliardi, Chem. Sci. **10**, 1716 (2019).
[24] E. G. Hohenstein, N. Luehr, I. S. Ufimtsev, and T. J. Martínez, J. Chem. Phys. **142**, 224103 (2015).
[25] J. W. Snyder, B. F. Curchod, and T. J. Martínez, J. Phys. Chem. Lett. **7**, 2444 (2016).
[26] J. Olsen, B. O. Roos, P. Jo/rgensen, and H. J. A. Jensen, J. Chem. Phys. **89**, 2185 (1988).
[27] P. Å. Malmqvist, A. Rendell, and B. O. Roos, J. Phys. Chem. **94**, 5477 (1990).
[28] D. Ma, G. Li Manni, and L. Gagliardi, J. Chem. Phys. **135**, 044128 (2011).
[29] J. Ivanic, J. Chem. Phys. **119**, 9364 (2003).
[30] S. M. Parker, T. Seideman, M. A. Ratner, and T. Shiozaki, J. Phys. Chem. C **118**, 12700 (2014).
[31] S. Nishio and Y. Kurashige, J. Chem. Phys. **151**, 084111 (2019).
[32] R. K. Kathir, C. de Graaf, R. Broer, and R. W. A Havenith, J. Chem. Theory Comput. (2020), 10.1021/acs.jctc.9b01144.
[33] M. R. Hermes and L. Gagliardi, J. Chem. Theory Comput. **15**, 972 (2019).
[34] R. Pandharkar, M. R. Hermes, C. J. Cramer, and L. Gagliardi, J. Phys. Chem. Lett. **10**, 5507 (2019).
[35] M. R. Hermes, R. Pandharkar, and L. Gagliardi, J. Chem. Theory Comput. **16**, 4923 (2020).
[36] R. Pandharkar, M. R. Hermes, C. J. Cramer, D. G. Truhlar, and L. Gagliardi, J. Chem. Theory Comput. **17**, 2843 (2021).
[37] C. A. Jiménez-Hoyos and G. E. Scuseria, Phys. Rev. B **92**, 085101 (2015).
[38] V. Abraham and N. J. Mayhall, J. Chem. Theory Comput. **16**, 6098 (2020).
[39] A. Papastathopoulos-Katsaros, C. A. Jiménez-Hoyos, T. M. Henderson, and G. E. Scuseria, "A cluster-based mean-field, perturbative and coupled-cluster theory description of strongly correlated systems," (2021).
[40] Q. Wang, M. Duan, E. Xu, J. Zou, and S. Li, J. Phys. Chem. Lett. **11**, 7536 (2020).
[41] D. I. Lyakh, M. Musiał, V. F. Lotrich, and R. J. Bartlett, Chem. Rev. **112**, 182 (2012).
[42] C. Møller and M. S. Plesset, Phys. Rev. **46**, 618 (1934).
[43] I. Shavitt and R. J. Bartlett, *Many-Body Methods in Chemistry and Physics* (Cambridge University Press, Cambridge, U.K., 2009).
[44] Y. Cao, J. Romero, J. P. Olson, M. Degroote, P. D. Johnson, M. Kieferová, I. D. Kivlichan, T. Menke, B. Peropadre, N. P. Sawaya, *et al.*, Chem. Rev. **119**, 10856 (2019).
[45] K. Head-Marsden, J. Flick, C. J. Ciccarino, and P. Narang, Chem. Rev. **121**, 3061 (2020).
[46] S. McArdle, S. Endo, A. Aspuru-Guzik, S. C. Benjamin, and X. Yuan, Rev. Mod. Phys. **92**, 015003 (2020).
[47] S. Lloyd, Science , 1073 (1996).
[48] A. Y. Kitaev, arXiv preprint quant-ph/9511026 (1995).
[49] D. S. Abrams and S. Lloyd, Phys. Rev. Lett. **83**, 5162 (1999).
[50] A. Y. Kitaev, A. Shen, M. N. Vyalyi, and M. N. Vyalyi, *Classical and quantum computation*, 47 (American Mathematical Soc., 2002).
[51] B. O'Gorman, S. Irani, J. Whitfield, and B. Fefferman, arXiv preprint arXiv:2103.08215 (2021).
[52] J. Romero, R. Babbush, J. R. McClean, C. Hempel, P. J. Love, and A. Aspuru-Guzik, Quantum Sci. Technol. **4**, 014008 (2018).
[53] A. Peruzzo, J. McClean, P. Shadbolt, M.-H. Yung, X.-Q. Zhou, P. J. Love, A. Aspuru-Guzik, and J. L. O'brien, Nat. Commun. **5**, 1 (2014).
[54] J. Preskill, Quantum **2**, 79 (2018).
[55] D. Wecker, M. B. Hastings, and M. Troyer, Phys. Rev. A **92**, 042303 (2015).
[56] J. R. McClean, M. E. Kimchi-Schwartz, J. Carter, and W. A. De Jong, Phys. Rev. A **95**, 042308 (2017).
[57] A. Kandala, A. Mezzacapo, K. Temme, M. Takita, M. Brink, J. M. Chow, and J. M. Gambetta, Nature **549**, 242 (2017).
[58] T. Fleig, J. Olsen, and C. M. Marian, J. Chem. Phys. **114**, 4775 (2001).
[59] J. Li, Y. Yao, A. A. Holmes, M. Otten, Q. Sun, S. Sharma, and C. Umrigar, Phys. Rev. Res. **2**, 012015 (2020).
[60] J. Li, M. Otten, A. A. Holmes, S. Sharma, and C. J. Umrigar, J. Chem. Phys. **149**, 214110 (2018).
[61] R. Olivares-Amaya, W. Hu, N. Nakatani, S. Sharma, J. Yang, and G. K.-L. Chan, J. Chem. Phys. **142**, 034102 (2015).
[62] S. Knecht, E. D. Hedegård, S. Keller, A. Kovyrshin, Y. Ma, A. Muolo, C. J. Stein, and M. Reiher, arXiv preprint arXiv:1512.09267 (2015), 10.2533/chimia.2016.244.
[63] Y. Kurashige and T. Yanai, J. Chem. Phys. **135**, 094104 (2011).
[64] K. H. Marti and M. Reiher, in *Progress in Physical Chemistry Volume 3* (Oldenbourg Wissenschaftsverlag, 2011) pp. 293–309.
[65] A. Bernhardsson, R. Lindh, J. Olsen, and M. Fulscher, Mol. Phys. **96**, 617 (1999).
[66] J. Stålring, A. Bernhardsson, R. Lindh, J. Stalring, A. Bernhardssont, and R. Lindhf, Mol. Phys. **99**, 103 (2001).
[67] M. R. Hoffmann and J. Simons, J. Chem. Phys. **88**, 993 (1988).
[68] Q. Sun and G. K. L. Chan, J. Chem. Theory Comput. **10**, 3784 (2014).
[69] B. Bauer, S. Bravyi, M. Motta, and G. K.-L. Chan, Chem. Rev. **120**, 12685 (2020).
[70] M. Murugesu, M. Habrych, W. Wernsdorfer, K. A. Abboud, and G. Christou, J. Am. Chem. Soc. **126**, 4766 (2004), pMID: 15080666, https://doi.org/10.1021/ja0316824.
[71] A. Baniodeh, N. Magnani, Y. Lan, G. Buth, C. E. Anson, J. Richter, M. Affronte, J. Schnack, and A. K. Powell, npj Quantum Mater. **3**, 1 (2018).
[72] M. B. Smith and J. Michl, Annu. Rev. Phys. Chem. **64**, 361 (2013).

[73] D. Casanova, Chem. Rev. **118**, 7164 (2018).

[74] F. A. Evangelista, G. K.-L. Chan, and G. E. Scuseria, J. Chem. Phys. **151**, 244112 (2019), https://doi.org/10.1063/1.5133059.

[75] F. Arute, K. Arya, R. Babbush, D. Bacon, J. C. Bardin, R. Barends, S. Boixo, M. Broughton, B. B. Buckley, D. A. Buell, B. Burkett, N. Bushnell, Y. Chen, Z. Chen, B. Chiaro, R. Collins, W. Courtney, S. Demura, A. Dunsworth, E. Farhi, A. Fowler, B. Foxen, C. Gidney, M. Giustina, R. Graff, S. Habegger, M. P. Harrigan, A. Ho, S. Hong, T. Huang, W. J. Huggins, L. Ioffe, S. V. Isakov, E. Jeffrey, Z. Jiang, C. Jones, D. Kafri, K. Kechedzhi, J. Kelly, S. Kim, P. V. Klimov, A. Korotkov, F. Kostritsa, D. Landhuis, P. Laptev, M. Lindmark, E. Lucero, O. Martin, J. M. Martinis, J. R. McClean, M. McEwen, A. Megrant, X. Mi, M. Mohseni, W. Mruczkiewicz, J. Mutus, O. Naaman, M. Neeley, C. Neill, H. Neven, M. Y. Niu, T. E. O'Brien, E. Ostby, A. Petukhov, H. Putterman, C. Quintana, P. Roushan, N. C. Rubin, D. Sank, K. J. Satzinger, V. Smelyanskiy, D. Strain, K. J. Sung, M. Szalay, T. Y. Takeshita, A. Vainsencher, T. White, N. Wiebe, Z. J. Yao, P. Yeh, and A. Zalcman, Science **369**, 1084 (2020), https://www.science.org/doi/pdf/10.1126/science.abb9811.

[76] A. J. McCaskey, Z. P. Parks, J. Jakowski, S. V. Moore, T. D. Morris, T. S. Humble, and R. C. Pooser, npj Quantum Inf. **5**, 1 (2019).

[77] P. J. J. O'Malley, R. Babbush, I. D. Kivlichan, J. Romero, J. R. McClean, R. Barends, J. Kelly, P. Roushan, A. Tranter, N. Ding, B. Campbell, Y. Chen, Z. Chen, B. Chiaro, A. Dunsworth, A. G. Fowler, E. Jeffrey, E. Lucero, A. Megrant, J. Y. Mutus, M. Neeley, C. Neill, C. Quintana, D. Sank, A. Vainsencher, J. Wenner, T. C. White, P. V. Coveney, P. J. Love, H. Neven, A. Aspuru-Guzik, and J. M. Martinis, Phys. Rev. X **6**, 031007 (2016).

[78] N. M. Tubman, C. Mejuto-Zaera, J. M. Epstein, D. Hait, D. S. Levine, W. Huggins, Z. Jiang, J. R. McClean, R. Babbush, M. Head-Gordon, *et al.*, arXiv preprint arXiv:1809.05523 (2018).

[79] K. Sugisaki, S. Nakazawa, K. Toyota, K. Sato, D. Shiomi, and T. Takui, ACS central science **5**, 167 (2018).

[80] H. R. Grimsley, S. E. Economou, E. Barnes, and N. J. Mayhall, Nat. Commun. **10**, 1 (2019).

[81] M. Cerezo, A. Arrasmith, R. Babbush, S. C. Benjamin, S. Endo, K. Fujii, J. R. McClean, K. Mitarai, X. Yuan, L. Cincio, *et al.*, Nat. Rev. Phys. , 1 (2021).

[82] K. Bharti, A. Cervera-Lierta, T. H. Kyaw, T. Haug, S. Alperin-Lea, A. Anand, M. Degroote, H. Heimonen, J. S. Kottmann, T. Menke, *et al.*, arXiv preprint arXiv:2101.08448 (2021).

[83] D. A. Fedorov, Y. Alexeev, S. K. Gray, and M. Otten, arXiv preprint arXiv:2109.12652 (2021).

[84] E. Neuscamman, T. Yanai, and G. K.-L. Chan, Int. Rev. Phys. Chem. **29**, 231 (2010).

[85] P. W. Shor, SIAM Review **41**, 303 (1999).

[86] A. W. Harrow, A. Hassidim, and S. Lloyd, Phys. Rev. Lett. **103**, 150502 (2009).

[87] P. Shor, in *Proceedings 35th Annual Symposium on Foundations of Computer Science* (1994) pp. 124–134.

[88] G. Ortiz, J. E. Gubernatis, E. Knill, and R. Laflamme, Phys. Rev. A **64**, 022319 (2001).

[89] R. Babbush, J. McClean, D. Wecker, A. Aspuru-Guzik, and N. Wiebe, Phys. Rev. A **91**, 022311 (2015).

[90] D. W. Berry, A. M. Childs, R. Cleve, R. Kothari, and R. D. Somma, Phys. Rev. Lett. **114**, 090502 (2015).

[91] G. H. Low and I. L. Chuang, Quantum **3**, 163 (2019).

[92] P. Jordan and E. P. Wigner, in *The Collected Works of Eugene Paul Wigner* (Springer, 1993) pp. 109–129.

[93] S. Bravyi, J. M. Gambetta, A. Mezzacapo, and K. Temme, arXiv preprint arXiv:1701.08213 (2017).

[94] S. B. Bravyi and A. Y. Kitaev, Ann. Phys. **298**, 210 (2002).

[95] V. E. Elfving, B. W. Broer, M. Webber, J. Gavartin, M. D. Halls, K. P. Lorton, and A. Bochevarov, arXiv preprint arXiv:2009.12472 (2020).

[96] H. Liu, G. H. Low, D. S. Steiger, T. Häner, M. Reiher, and M. Troyer, arXiv preprint arXiv:2102.10081 (2021).

[97] I. H. Kim, E. Lee, Y.-H. Liu, S. Pallister, W. Pol, and S. Roberts, arXiv preprint arXiv:2104.10653 (2021).

[98] R. J. Bartlett, S. A. Kucharski, and J. Noga, Chem. Phys. Lett. **155**, 133 (1989).

[99] A. G. Taube and R. J. Bartlett, Int. J. Quantum Chem. **106**, 3393 (2006).

[100] W. Kutzelnigg, Theor. Chim. Acta **80**, 349 (1991).

[101] Y. Shen, X. Zhang, S. Zhang, J.-N. Zhang, M.-H. Yung, and K. Kim, Phys. Rev. A **95**, 020501 (2017).

[102] G. Harsha, T. Shiozaki, and G. E. Scuseria, J. Chem. Phys. **148**, 044107 (2018), https://doi.org/10.1063/1.5011033.

[103] M. R. Hermes, "https://github.com/MatthewRHermes/mrh," (2018).

[104] J. Chen, H.-P. Cheng, and J. Freericks, J. Chem. Theory Comput. **17**, 841 (2021), arXiv:2008.06637.

[105] K. Svore, A. Geller, M. Troyer, J. Azariah, C. Granade, B. Heim, V. Kliuchnikov, M. Mykhailova, A. Paz, and M. Roetteler, in *Proceedings of the Real World Domain Specific Languages Workshop 2018* (2018) pp. 1–10.

[106] G. H. Low, N. P. Bauman, C. E. Granade, B. Peng, N. Wiebe, E. J. Bylaska, D. Wecker, S. Krishnamoorthy, M. Roetteler, K. Kowalski, *et al.*, arXiv preprint arXiv:1904.01131 (2019).

arXiv:2203.02012v1 [quant-ph] 3 Mar 2022

Supplementary Information for Localized Quantum Chemistry on Quantum Computers

Matthew Otten,[1,*] Matthew R. Hermes,[2] Riddhish Pandharkar,[2] Yuri Alexeev,[3] Stephen K. Gray,[4] and Laura Gagliardi[5]

[1]*HRL Laboratories, LLC, 3011 Malibu Canyon Road, Malibu, CA 90265*
[2]*Department of Chemistry, Pritzker School of Molecular Engineering, James Franck Institute, Chicago Center for Theoretical Chemistry, University of Chicago, Chicago, IL 60637, USA.*
[3]*Computational Science Division, Argonne National Laboratory, Lemont, IL 60439, USA*
[4]*Center for Nanoscale Materials, Argonne National Laboratory, Lemont, IL 60439, USA*
[5]*Department of Chemistry, Pritzker School of Molecular Engineering, James Franck Institute, Chicago Center for Theoretical Chemistry, University of Chicago, Chicago, IL 60637; Argonne National Laboratory, Lemont, IL 60439, USA.*

(Dated: March 7, 2022)

I. LAS-VQE

Here we describe a more approximate approach than LAS-UCC wherein the QPE circuits for the fragments are replaced by UCC ansatzes, leading to a fully variational method. The chemical knowledge that guides us in defining subspaces of the LAS wave function can also be used to reduce the size of the unitary operator for the UCC ansatzes. It suggests that operators corresponding to the higher excitation from one fragment to another do not affect the wave function significantly. Thus, we introduce a modified ansatz for truncated UCC circuits where we consider the "locality" of the excitation. An excitation involving only orbitals localized on a particular fragment—that is defined by the user—is classified as a "local excitation." In this modified UCC ansatz the user not only can truncate the UCC excitation to a certain maximum number (doubles, triples, etc.) but also can impose a constraint of locality on the higher excitations. We develop here the theory and the algorithm of this method and name it LAS-VQE. In LAS-VQE, all the singles excitations are included while only the local ones are included for the higher excitations. This corresponds to having a mean-field interfragment interaction and allowing all possible orbital rotations. This does not reduce the number of qubits required to represent the system, but it does lower the complexity of the circuit as discussed below. In principle, one could use the locality argument to include only local excitations, allowing us to reduce the number of qubits required. This separate-fragments VQE approach, however, fails to account for any interaction between the fragments. We choose to always include the singles excitations (orbital rotations) across the entire system to account for some interfragment correlation and to make the method less sensitive to the localization schemes used.

We also choose to perform in the singles excitation among spin-restricted orbitals. We achieve this by using the same parameter to control the alpha and beta excitations corresponding to a given pair of spatial orbitals. This is necessary to avoid artificial lowering of energies due to spontaneous symmetry breaking (the spin unrestricted solution). An example of the effect of this is seen for the hydrogen dimer shown in Figure 2 of the main text. The nonspin adapted UCCS energy is about 0.2 mHartree lower than the Hartree–Fock and has an spin contamination of 0.09, showing the symmetry breaking. Working with spin-restricted orbitals not only allows us to prepare symmetry preserving states for the subsequent excitations, but also lowers the number of parameters at the singles level by a factor of 2. This becomes a significant advantage for the classical optimizer in VQE as the size of the system gets larger. We study the ground state electronic structure of the hydrogen dimer in various conformations with the STO-3G basis set. We use CASSCF with a (4,4) active space and LASSCF with a ((2,2),(2,2)) active space, UCCSD and LAS-VQE. Each H_2 molecule is considered as one fragment on which the molecular orbitals are localized. As one would expect, the performance of LASSCF with respect to CASSCF (which is also FCI in this case) worsens with decreasing distance between the two H_2 molecules. Figure 1 shows the energy difference between the various methods and

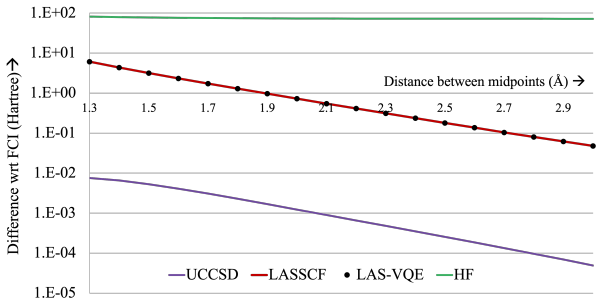


FIG. 1. Energy difference (in Hartree) between FCI and the approximate methods as a function of the distance between the midpoints of the two H_2 molecules

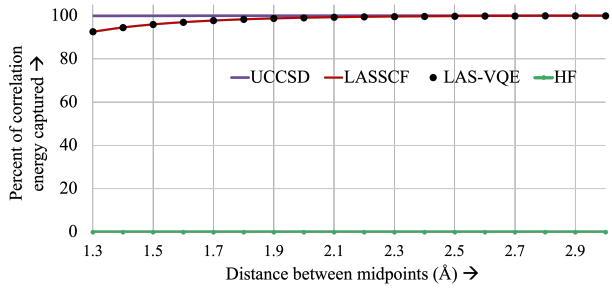


FIG. 2. Percentage of correlation energy accounted for by the various methods for different intermolecular distances

the FCI/CAS(4,4) absolute energies. UCCSD in this case is not exactly FCI but does give accurate results. LAS-VQE is close to (but slightly lower than) the LASSCF energy. The LAS-VQE energy is not variationally bound by the LASSCF that it is based on. In contrast to the LAS-UCC method discussed in this paper, this method uses a single determinant Hartree–Fock reference state. The UCCSD energy is a variational lower bound to the LAS-VQE method. There is, however, a significant advantage when it comes to the computational cost: gate count and the depth of the circuit. The number of doubles operators scales linearly with the number of fragments. The Table I shows the number of gates and parameters required for the various calculations for a system with increasing number of H_2 molecules with the same fragmentation scheme. LAS-VQE in considerably lower in both circuit depth and number of parameters, compared with full UCCSD.

TABLE I. Circuit depth and number of parameters for the various methods for an increasing number of H_2 fragments

	Circuit Depth			Parameters		
	UCCS	LAS-VQE	UCCSD	UCCS	LAS-VQE	UCCSD
$1 \times H_2$	14	97	97	1	2	2
$2 \times H_2$	58	141	1791	4	6	22
$3 \times H_2$	147	230	11206	9	12	108
$4 \times H_2$	296	379	42789	16	20	344

II. JUSTIFICATION OF EQ. (9) OF THE MAIN TEXT

Substituting Eqs. (4) and (6) into the Eq. (3) of the main text and differentiating with respect to generator amplitude $x_{\vec{k}}$ yields

$$\frac{\partial E_{\mathrm{LAS}}}{\partial x_{\vec{k}}} = \langle\Phi| \bigwedge_{L\neq K} \langle\Psi_L| \wedge \langle\vec{k}|\hat{H} - E_{\mathrm{LAS}}|\Psi_K\rangle \bigwedge_{M\neq K} |\Psi_M\rangle \wedge |\Phi\rangle\,, \tag{1}$$

the vanishing of which corresponds to the minimization of the LAS energy given by Eq. (3). Within the Hilbert space of the Kth fragment, the energy minimization conditions for the $x_{\vec{k}}$ amplitudes corresponds to an eigenproblem,

$$\hat{H}_K\,|\Psi_K\rangle = E_{\mathrm{LAS}}\,|\Psi_K\rangle\,, \tag{2}$$

where

$$\begin{aligned}\hat{H}_K &\equiv \langle\Phi| \bigwedge_{L\neq K} \langle\Psi_L|\,\hat{H} \bigwedge_{M\neq K} |\Psi_M\rangle \wedge |\Phi\rangle \\ &= \tilde{h}^{k_1}_{k_2}\hat{a}^\dagger_{k_1}\hat{a}_{k_2} + \frac{1}{4}h^{k_1k_3}_{k_2k_4}\hat{a}^\dagger_{k_1}\hat{a}^\dagger_{k_3}\hat{a}_{k_4}\hat{a}_{k_2},\end{aligned} \tag{3}$$

where $\tilde{h}^{k_1}_{k_2}$ is given by Eq. (10) of the main text. This effective Hamiltonian describes the Kth fragment without interacting with any other fragment; $\hat{H}_K$ for various K mutually commute.

For a system composed of noninteracting fragments A and B with Hamiltonians $\hat{H}_A$ and $\hat{H}_B$, energies E_A and E_B, and wave functions $|\Psi_A\rangle$ and $|\Psi_B\rangle$, it is generally true that

$$\left(\hat{H}_A + \hat{H}_B\right)|\Psi_A\rangle \wedge |\Psi_B\rangle = (E_A + E_B)\,|\Psi_A\rangle \wedge |\Psi_B\rangle\,. \tag{4}$$

Noting that $\hat{H}_{\mathrm{eff}}$ given by Eq. (9) of the main text is obviously

$$\hat{H}_{\mathrm{eff}} = \sum_K \hat{H}_K, \tag{5}$$

we conclude that

$$\hat{H}_{\mathrm{eff}} \bigwedge_K |\Psi_K\rangle = n_f \times E_{\mathrm{LAS}} \bigwedge_K |\Psi_K\rangle\,. \tag{6}$$

In other words, $\hat{H}_{\mathrm{eff}}$ models interacting fragments as non-interacting subsystems described by unrelated, mutually commuting effective Hamiltonian terms. Thus, the QPE algorithm applied to $\hat{H}_{\mathrm{eff}}$ generates $|\mathrm{QLAS}\rangle \equiv \bigwedge_K |\Psi_K\rangle$ on the quantum circuit.

III. ORBITAL ORDERING AND THE JORDAN-WIGNER TRANSFORMATION

The Jordan-Wigner transformation[1] is one of the many ways of transforming fermion operators into spin operators, and is a necessary step for performing quantum chemistry calculations on quantum computers. Here, we very briefly discuss the overheads associated with the Jordan-Wigner transformation and how it can be mitigated in certain fragmented geometries.

The Jordan-Wigner transformation transforms a fermion creation operator for orbital j, $a^\dagger_j$, out of a total of N spin orbitals as follows

$$\tilde{a}^\dagger_j = Z^{\otimes j-1} \otimes \frac{X - iY}{2} \otimes I^{\otimes N-1}, \tag{7}$$

where $\tilde{a}^\dagger_j$ is the transformed operator; X, Y, and Z are the Pauli operators; and the notation $Z^{\otimes N}$ denotes applying the tensor operation, $\otimes$, N times for Z (i.e., $Z^{\otimes 4} = Z\otimes Z\otimes Z\otimes Z$. The term $Z^{\otimes j-1}$ ensures that the transformed operators obey the correct fermionic anti-commutation relations. In standard quantum algorithms for quantum chemistry, these Z strings introduce very high-weight (that is, having many terms that are not I) terms into the Hamiltonian and cluster operators, leading to an $O(N)$ overhead. To see this, we focus on just the one-body terms. Under the Jordan-Wigner transformation, and assuming $j > k$,

$$\tilde{a}^\dagger_j\tilde{a}_k = I^{\otimes k-1} \otimes \frac{Z(X - iY)}{2} \otimes Z^{\otimes j-k-1} \otimes \frac{X - iY}{2} \otimes I^{\otimes N-j}. \tag{8}$$

The weight (number of non-identity terms) of this operator is $j-k+1$. In the most general case, there will exist terms where spin orbital 1 and N will have a nonzero component, and the resulting weight is N, which introduces the $O(N)$ overhead normally associated with the Jordan-Wigner transformation. There are many techniques for generally reducing this overhead[2,3]. In our simple chain of H_2 molecules, we can remove this scaling by choosing a particular ordering of the orbitals. One typical ordering of the orbitals is the following: all occupied spin up orbitals, all virtual spin up orbitals, all occupied spin down orbital, all virtual spin down orbitals. If this ordering is followed when using the local actives spaces of each

fragment, the $O(N)$ overhead is still applicable. Take, for example, just the one-body term from the first occupied spin up orbital of the first fragment to the first virtual spin up orbital for the first fragment. In this case, $j = 1$ and $k = O(N)$, leading to the typical $O(N)$ Jordan-Wigner scaling. If, instead, the orbitals are ordered with all occupied spin up orbitals of fragment one, followed by all virtual spin up orbitals of fragment one, followed the same for the second fragment, and so on, the overhead is removed. Now, $j = 1$ and $k = O(N_k)$, where N_k is the number of spin orbitals in each fragment. Since N_k is assumed to be fixed as the number of fragments grows, the $O(N)$ scaling is reduced to a constant. To remove the Jordan-Wigner overhead from mixed spin two-body terms, the ordering can be further changed so that each spin up orbital is immediately followed by its analogous spin down orbital. This shows that the Jordan-Wigner $O(N)$ overhead can be removed from all terms in the reduced Hamiltonian, removing the $O(N)$ scaling from the QPE part of LAS-UCC. For UCCSD correlators, the Jordan-Wigner overhead can be removed for certain geometries, such as the linear H_2 chain studied in the main text. More complex geometries, such as higher dimensional lattices, will re-introduce scaling terms, as the orbitals cannot be simultaneously ordered to give low-weight Pauli strings for terms which couple both in the multiple dimensions, such as x and y in a 2D lattice.

IV. SINGLE QUBIT ROTATION GATES

Figure 3 shows the estimated number of arbitrary single qubit rotation gates needed to implement full QPE across the whole molecule, the fragmented LAS-QPE, full UCCSD, and the 2-local UCCSD correlator with increasing number of H_2 molecules. Just like in the main text, LAS-UCC has polynomially fewer gates, compared with QPE or UCCSD, scaling only linearly for the linear chain geometry. QPE and UCCSD only need $O(N^4)$ single qubit rotations because the Jordan-Wigner overhead only shows up in the CNOT gates.

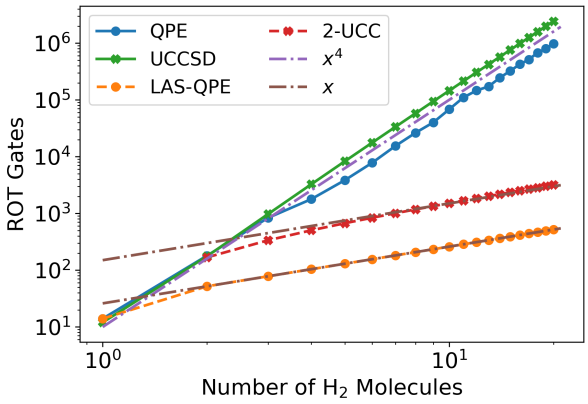


FIG. 3. Estimated single qubit arbitrary rotation gate counts using various algorithms. The QPE estimates assume only a single Trotter step. Polynomials of various orders have been plotted to demonstrate the scaling. Our algorithm, LAS-UCC, requires both the LAS-QPE and 2-UCC circuits and thus has an overall $O(N)$ scaling, compared with the $O(N^4)$ scaling of UCC and QPE.

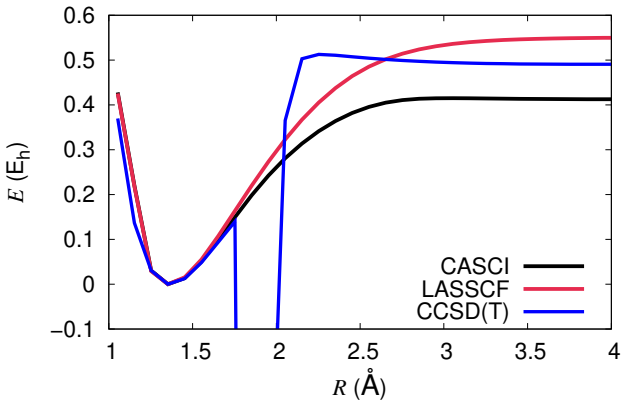


FIG. 4. Potential energy curve of the *trans*-butadiene molecule along the symmetric double C=C bond dissociation coordinate, computed with CASCI, LASSCF, and CCSD(T). Total energies for each method are shifted to zero at the equilibrium geometry.

V. STRONG CORRELATION OF *TRANS*-BUTADIENE

The symmetric double-bond dissociation curve of the *trans*-butadiene molecule (cf. Figs. 2b and 4 of the main text) calculated using the CCSD(T) method is plotted in Fig. 4 and compared to CASCI and LASSCF curves. In the dissociation limit, in which the molecule objectively can be modeled as three non-interacting diradical fragments, the CCSD(T) method recovers a greater amount of correlation energy than LASSCF, *albeit* not as much as LAS-UCC or CASCI. Near the equilibrium geometry, the three methods are indistinguishable.

However, unlike LASSCF, CASCI, or LAS-UCC, all of which are multireference methods, the single-reference CCSD(T) method cannot smoothly connect the region of the equilibrium geometry to the bond dissociation limit. The discontinuous and unphysical behavior of CCSD(T) in the region of $R = 1.8$Å is consistent with the tendency of single-reference coupled cluster at low truncation orders to struggle to dissociate multiple or high-order bonds.[4] This *trans*-butadiene potential energy curve is an example of a system in which both static and dynamical correlation must simultaneously be accounted for in order to obtain quantitatively accurate results.

VI. UCCSD OPERATOR ORDERING IN LAS-UCC

The following listings from the *mrh* package describe the operator order for the first-order Trotterized UCCSD correlator used in our classical LAS-UCC calculations. Individual spatial orbitals are indexed first by fragment, and then in decreasing order of their natural orbital occupancy

(before application of the UCCSD correlator). Listing 1 contains the code for generating the combinations of spatial-orbital excitation patterns, as well as a docstring summarizing the effects of the code presented in Listings 2 and 3 for the case of UCCSD. Listings 2 and 3 contain the code for generating valid spin-orbital excitation patterns for any general set of spatial-orbital excitation patterns of any order in a UCC operator. Note that "np" is numpy and "combinations_with_replacement" is from the itertools module. This code is from the commit identified by the SHA-1 hash 8bb3c2d46ab5f43c8787a365b22713b5410855f2, which differs from the commit which performed the calculations reported in the main text (fe564cd1c54c404edf8bce1dd7118b2d53acdd7a) only in docstrings, test scripts, and line wrapping.

For the UCCSD runs of the main text, Fig. (4), we use ordering consistent with Qiskit's UCCSD generation. We have included a short code listing (Listing 4) which will reproduce the excitation ordering.

* mjotten@hrl.com

[1] P. Jordan and E. P. Wigner, in *The Collected Works of Eugene Paul Wigner* (Springer, 1993) pp. 109–129.

[2] A. Tranter, P. J. Love, F. Mintert, and P. V. Coveney, Journal of Chemical Theory and Computation **14**, 5617 (2018).

[3] V. c. v. Havlíček, M. Troyer, and J. D. Whitfield, Phys. Rev. A **95**, 032332 (2017).

[4] X. Li and J. Paldus, J. Chem. Phys. **115**, 5774 (2001).

Listing 1. Code for generating the spatial-orbital list of the UCCSD correlator in LAS-UCC within *mrh*

```
def get_uccsd_op (norb, t1=None, t2=None):
    ''' Construct and optionally initialize semi-spin-adapted unitary CC
        correlator with singles and doubles spanning a single undifferentiated
        orbital range. Excitations from spatial orbital(s) i(, j) to spatial
        orbital(s) a(, b) are applied to the ket in the order

        U|ket> = u^n(n-1)_nn u^n(n-1)_n(n-1) u^n(n-2)_nn ... u^11_22 u^11_21
                 ... u^n_(n-1) u^n_(n-2) ... u^3_2 u^3_1 u^2_1 |ket>

        where ^ indicates creation operators (a, b; rows) and _ indicates
        annihilation operators (i, j; columns). The doubles amplitudes are
        arbitrarily chosen in the upper-triangular space (a,b <= i,j), but the
        lower-triangular space is used for the individual double pairs
        (a > b, i > j) and for the singles amplitudes (a > i). In all cases,
        row-major ordering is employed.

        The spin cases of a given set of orbitals a, b, i, j are grouped
        together. For singles, spin-up (a) and spin-down (b) amplitudes are
        constrained to be equal and the spin-up operator is on the right (i.e.,
        is applied first). For doubles, the spin case order is

        u|ket> -> ^bb_bb ^ab_ab ^ab_ba ^ba_ab ^ba_ba ^aa_aa |ket>

        For spatial orbital cases in which the same index appears more than
        once, spin cases that correspond to nilpotent (eg., ^pp_qr ^aa_aa),
        undefined (eg., ^pq_pq ^ab_ab), or redundant (eg., ^pq_pq ^ab_ba)
        operators are omitted.

        Args:
            norb : integer
                Total number of spatial orbitals. (0.5 * #spinorbitals)

        Kwargs:
            t1 : ndarray of shape (norb,norb)
                Amplitudes at which to initialize the singles operators
            t2 : None
                NOT IMPLEMENTED. Amplitudes at which to initialize the doubles
                operators

        Returns:
            uop : object of class FSUCCOperator
                The callable UCCSD operator
    '''
    t1_idx = np.tril_indices (norb, k=-1)
    ab_idxs, ij_idxs = list (t1_idx[0]), list (t1_idx[1])
    pq = [(p, q) for p, q in zip (*np.tril_indices (norb))]
    for ab, ij in combinations_with_replacement (pq, 2):
        ab_idxs.append (ab)
        ij_idxs.append (ij)
    uop = FSUCCOperator (norb, ab_idxs, ij_idxs)
    x0 = uop.get_uniq_amps ()
    if t1 is not None: x0[:len (t1_idx[0])] = t1[t1_idx]
    if t2 is not None: raise NotImplementedError ("t2 initialization")
    uop.set_uniq_amps_(x0)
    return uop
```

Listing 2. Code for generating spin-orbital excitation operators of UCC(SD) in *mrh*. The function "spincases" is presented in Listing 3

```
class FSUCCOperator (uccsd_sym0.FSUCCOperator):
    ''' A callable spin-adapted (Sz only) unrestricted coupled cluster
        operator. For single-excitation operators, spin-up and spin-down
        amplitudes are constrained to be equal. All spin cases for a given
        spatial-orbital excitation pattern (from i_idxs to a_idxs) are grouped
        together and applied to the ket in ascending order of the index

        (a_spin) * nelec + i_spin

        where 'a_spin' and 'i_spin' are the ordinal indices of the spin
        cases returned by the function 'spincases' for a_idxs (creation
        operators) and i_idxs (annihilation operators) respectively, and nelec
        is the order of the generator (1=singles, 2=doubles, etc.) Nilpotent
        or undefined spin cases (i.e., because of spatial-orbital index
        collisions) are omitted.
        '''


    def __init__(self, norb, a_idxs, i_idxs):
        # Up to two equal indices in one generator are allowed
        # However, we still can't have any equal generators
        self.a_idxs = []
        self.i_idxs = []
        self.symtab = []
        for ix, (a, i) in enumerate (zip (a_idxs, i_idxs)):
            a = np.ascontiguousarray (a, dtype=np.uint8)
            i = np.ascontiguousarray (i, dtype=np.uint8)
            errstr = 'a,i={},{} invalid for number-sym op'.format (a,i)
            assert (len (a) == len (i)), errstr
            #errstr = 'a,i={},{} degree of freedom undefined'.format (a,i)
            #assert (not (np.all (a == i))), errstr
            if len (a) == 1: # Only case where I know the proper symmetry
                             # relation between amps to ensure S**2
                symrow = [len (self.a_idxs), len (self.i_idxs)+1]
                self.a_idxs.extend ([a, a+norb])
                self.i_idxs.extend ([i, i+norb])
                self.symtab.append (symrow)
            else:
                for ix_ab, (ab, ma) in enumerate (zip (*spincases (a, norb))):
                    if np.amax (np.unique (ab, # nilpotent escape
                            return_counts=True)[1]) > 1: continue
                    for ix_ij, (ij, mi) in enumerate (zip (*spincases (
                            i, norb))):
                        if mi != ma: continue # sz-break escape
                        if np.all (ab==ij): continue # undefined escape
                        if np.all (a==i) and ix_ab>ix_ij:
                            continue # redundant escape
                        if np.amax (np.unique (ij, return_counts=True)[1]) > 1:
                            continue # nilpotent escape
                        self.symtab.append ([len (self.a_idxs)])
                        self.a_idxs.append (ab)
                        self.i_idxs.append (ij)
        self.norb = 2*norb
        self.ngen = len (self.a_idxs)
        assert (len (self.i_idxs) == self.ngen)
        self.uniq_gen_idx = np.array ([x[0] for x in self.symtab])
        self.amps = np.zeros (self.ngen)
        self.assert_sanity ()
```

Listing 3. Code for generating a valid list of spin cases corresponding to a set of field operators for particular spatial orbitals in *mrh*

```
def spincases (p_idxs, norb):
    ''' Compute the spinorbital indices corresponding to all spin cases of a
        set of field operators acting on a specified list of spatial orbitals
        The different spin cases are returned 'column-major order':

        aaa...
        baa...
        aba...
        bba...
        aab...

        The index of a given spincase string ('aba...', etc.) can be computed
        as

        p_spin = int (spincase[::-1].replace ('a','0').replace ('b','1'), 2)

        Args:
            p_idxs : ndarray of shape (nelec,)
                Spatial orbital indices
            norb : integer
                Total number of spatial orbitals

        Returns:
            p_idxs : ndarray of shape (2^nelec, nelec)
                Rows contain different spinorbital cases of the input spatial
                orbitals
            m : ndarray of shape (2^nelec,)
                Number of beta (spin-down) orbitals in each spin case
    '''
    nelec = len (p_idxs)
    p_idxs = p_idxs[None,:]
    m = np.array ([0])
    for ielec in range (nelec):
        q_idxs = p_idxs.copy ()
        q_idxs[:,ielec] += norb
        p_idxs = np.append (p_idxs, q_idxs, axis=0)
        m = np.append (m, m+1)
    p_sorted = np.stack ([np.sort (prow) for prow in p_idxs], axis=0)
    idx_uniq = np.unique (p_sorted, return_index=True, axis=0)[1]
    p_idxs = p_idxs[idx_uniq]
    m = m[idx_uniq]
    return p_idxs, m
```

Listing 4. Code for generating the excitation operators of the UCCSD ansatz for the UCCSD calculations of Fig. (4) of the main text.

```
def generate_fermionic_excitations_occ(num_excitations, num_spin_orbitals, num_particles,
                                       alpha_occ, alpha_unocc, beta_occ, beta_unocc):
    #Assumes ordering [occ_alpha, unocc_alpha, occ_beta, unocc_beta]
    alpha_excitations = []
    # generate alpha-spin orbital indices for occupied and unoccupied ones
    # the Cartesian product of these lists gives all possible single alpha-spin excitations
    alpha_excitations = list(itertools.product(alpha_occ, alpha_unocc))

    # the Cartesian product of these lists gives all possible single beta-spin excitations
    beta_excitations = list(itertools.product(beta_occ, beta_unocc))

    # we can find the actual list of excitations by doing the following:
    #   1. combine the single alpha- and beta-spin excitations
    #   2. find all possible combinations of length `num_excitations`
    pool = itertools.combinations(
        alpha_excitations + beta_excitations, num_excitations
    )

    excitations = list()
    visited_excitations = set()

    for exc in pool:
        # validate an excitation by asserting that all indices are unique:
        #   1. get the frozen set of indices in the excitation
        exc_set = frozenset(itertools.chain.from_iterable(exc))
        #   2. all indices must be unique (size of set equals 2 * num_excitations)
        #   3. and we palso don't want to include permuted variants of identical excitations
        if len(exc_set) == num_excitations * 2 and exc_set not in visited_excitations:
            visited_excitations.add(exc_set)
            occ, unocc = zip(*exc)
            exc_tuple = (occ, unocc)
            excitations.append(exc_tuple)

    return excitations
```